Journal of Colloid and Interface Science 409 (2013) 219–226

Contents lists available at ScienceDirect

Journal of Colloid and Interface Science

www.elsevier.com/locate/jcis

Conductive oxygen barrier films using supramolecular assembly of graphene embedded polyelectrolyte multilayers

Ankush A. Gokhale [a], Jue Lu [b], Nathan J. Parker [a], Andrew P. Izbicki [a], Oishi Sanyal [a], Ilsoon Lee [a,*]

[a] Department of Chemical Engineering and Materials Science, Michigan State University, East Lansing, MI 48824-1226, United States
[b] Technova Corporation, 1926 Turner Street, Lansing, MI 48906, United States

ARTICLE INFO

Article history:
Received 15 May 2013
Accepted 16 July 2013
Available online 30 July 2013

Keywords:
Graphene nanoplatelet
Gas barrier
Conductive films
Polyelectrolyte multilayers
Layer-by-layer assembly

ABSTRACT

The supramolecular self-assembly of polyelectrolyte multilayers (PEMs) provides robust bottom-up strategies to assemble a broad spectrum of nanostructures on the host substrates. In this study, we discuss the formation of graphene nanoplatelet (GNP) embedded polyelectrolyte films to enhance the oxygen barrier properties of poly(ethylene terephthalate) (PET) films. Despite cheaper costs and high mechanical strength, the diffusion of small gas molecules such as oxygen through PET films remains a matter of great concern. The simple yet robust supramolecular deposition of GNP/polyelectrolyte on PET substrates significantly increases the tortuous path the oxygen molecule has to travel, making it harder to diffuse through the PET film. With permeability coefficients in the range of 10–18 cc cm/cm^2 s Pa, the coatings developed in this study show three orders of magnitude reduction as compared to the permeability coefficient of the bare PET film, significantly lower than that of ethylene vinyl alcohol (EVOH) and comparable to silicon oxide thin films used in commercial gas barrier foils. The use of GNPs in the multilayered films also helped reduce the electrical sheet resistance to about 1 MΩ which is five orders of magnitude lower than the original PET substrate opening up promising opportunities for future use in semiconductor and electronics industry. Making suitable modifications in the deposition process, three configurations of GNP embedded PEM multilayers namely hydrogen bonded, electrostatic, and composite films were developed and their effect on oxygen barrier property and sheet resistance was monitored. Oxygen permeability of films was tested in accordance with ASTM D-3985 using a MOCON 2/21 ML instrument, whereas electrical sheet resistance was quantified using a Gamry Femtostat Electrochemical Impedance station.

1. Introduction

In recent years, there is a growing trend toward using flexible plastic as packaging material due to its low cost, easy formability, light weight, and reasonably good durability. Glass has been traditionally used in the food packaging industry and fabrication of display panels on account of its transparency, heat tolerance, and gas shielding capability [1]. However today, flexible plastics are making rapid inroads in replacing glass in most of these applications. In order to truly compete as an alternative packaging material, flexible plastic needs to fulfill an important requirement of preserving the product from environmental degradation. Dust, oxidation and moisture are principal forces in nature that can have a deleterious effect on perishable food products and sensitive electronic components [2]. Unfortunately, flexible plastics despite their numerous advantages suffer from poor gas barrier properties [3]. Efforts have been directed to overcome this problem by depositing inorganic coatings and thin films of polymer blends to improve the gas shielding capability. Among the inorganic materials, aluminum and silicon oxide coatings are excellent candidates to limit the permeation of gas molecules. However, inorganic coatings especially pure SiO_2 thin films require high temperature for effective deposition [4]. Most flexible plastics have low glass transition temperatures (T_g) imposing a limitation on the use of inorganic coatings.

Flexible plastics are positioned to make key contributions to the electronics industry in the near future. Devices such as organic light emitting diodes (OLED) expected to corner a 40% share of the mobile phone display market by 2015 present exciting growth prospects for the plastics industry [5]. With the world rapidly moving toward miniaturization, researchers have sought to make electronic components more compact by designing new prototypes that promote improved electrical conductivity and gas barrier properties. This would be particularly useful in the fabrication of certain semiconductor materials such as the dielectric constant oxides that are frequently used in the construction of large capacitors. These devices are liable to fail in the presence of non-conducting oxide coatings [6,7]. Other devices with similar conductive gas barrier requirements include solar cells grown on flexible supports and flat panel displays [8–10]. Silicon oxide though available ubiquitously, acts

* Corresponding author. Fax: +1 517 432 1105.
E-mail address: leeil@egr.msu.edu (I. Lee).

0021-9797/$ - see front matter © 2013 Elsevier Inc. All rights reserved.
http://dx.doi.org/10.1016/j.jcis.2013.07.036

as an electrical insulator [11]. So it cannot be directly applied for the above applications. In recent years, there has been a growing interest in the use of nanomaterials to supplement the gas barrier properties of thin polymer films. A number of theoretical models have been used to examine the critical role played by the aspect ratio of nano/colloidal materials dispersed in polymer matrix in improving the gas barrier properties [12–14]. Upon encountering a nanofiller, gas molecules are forced to adopt a tortuous pathway, producing a significant lag in the transmission. Therefore, high aspect ratio nanomaterials such as clay platelets [15–17], mica sheets [18,19], cellulose [20,21], and graphene oxide [22] have been used to build gas resistant thin films. In spite of their high gas/moisture barrier properties, these nanomaterials provide little advantage in the preparation of conductive films. On the other hand, graphene with its sp^2 hybridized 2D structure has unique physical and electronic properties [23]. Thin graphene layers are impermeable to most gases and could serve as excellent nanofillers in the polymer matrix [24]. High charge mobility and ballistic transport at room temperature endow graphene with superior electrical conductivity, making it a promising candidate for applications such as electrochemical sensing, field effect transistors (FET), and supercapacitors [25].

Layer-by-layer (LbL) assembly is a versatile technique that can be used to add multiple functionalities to a host of substrates. The success of the LbL technique lies in its ubiquity and simple operation. The extension of Iler's work [26] to the polyelectrolyte multilayer assembly by Decher and Hong [27,28] has given rise to a large number of nanoscopic functional materials. The non-covalent functionalization of nanomaterials using polyelectrolytes followed by sequential assembly is a form of LbL that has successfully demonstrated its utility. A number of interactions, such as electrostatic, hydrophobic, and hydrogen bonding, are ascribed to the formation of multilayered polyelectrolyte LbL assembly [29]. Multifunctional tailor-made substrates fabricated using this route have found several applications such as in catalysis [30–32], membrane science [33,34], biosensors [35–38], and drug delivery [39–42]. Ionic strength and pH of the solution can influence the adsorption process producing films of distinct morphology and properties [43–46].

With an estimated theoretical elastic modulus of single-layered graphene projected to be 1 TPa and surface conductivity about 50×10^6 S/cm, GNPs enjoy superior mechanical and electrical properties [47]. In recent years, methods such as thermal expansion, dielectric heating, and acid intercalation have facilitated exfoliation of graphitic flakes enabling the production of high surface area single-layered graphene nanoplatelets [48]. In this study, we report the LbL assembly of GNP embedded polyelectrolyte multilayers. Unlike inorganic coatings prepared under high temperature conditions, the GNP/PEM LbL assembly can be processed at room temperature. Similarly, compared to the recently developed fabrication methods for free standing graphite papers [49] and graphene nanoplatelet-high density polyethylene (GNP-HDPE) nanocomposite [50], the LbL process can be accomplished under milder process conditions using lower energy input. The GNP embedded polyelectrolyte films serve two purposes. Firstly, they serve as barriers to gas permeation. Secondly, graphene with its unique electronic configuration is positioned to deliver improved electrical conductance. The combination of gas barrier properties and electrical conductance make these films attractive candidates for applications in the semiconductor and electronics industry. Graphene dispersion in polyelectrolytes followed by its LbL assembly has been a subject of extensive examination [51,52]. Both strong and weak polyelectrolytes have been utilized for this purpose with varying degrees of success. While strong polyelectrolytes are fairly stable over a wide range of pH, weak polyelectrolytes are known to exhibit a remarkable variation in the charge distribution when subjected to a pH change [53]. This can affect the film thickness, the mechanism of interaction, the adsorption kinetics, and the quality of adhesion of the films to the base substrate. Unlike other studies that utilized graphene oxide followed by its reduction [54,55], our process did not use any oxidation or reduction steps. Instead, we chose two weak polyelectrolytes namely branched polyethylenimine (BPEI) and polyacrylic acid (PAA) for LbL deposition. BPEI is rich in amino pendant groups giving it a cationic character. The abundant availability of primary, secondary, and tertiary amino residues provides ample opportunities to use BPEI to complement the anionic carboxylic group rich PAA in a multilayered assembly. Using different process conditions, three sets of GNP embedded LbL assemblies were developed. They comprised of hydrogen bonding, electrostatic, and composite interactions (combination of hydrogen bonding and electrostatic interactions).

2. Experimental procedures

2.1. Materials

Polyacrylic acid (PAA) sodium salt (35 wt% solution in water) and branched polyethylenimine (BPEI) average $M_w \sim 25{,}000$ were purchased from Sigma Aldrich. Poly(ethylene terephthalate) (PET) films (Mylar A: thickness approximately 76.2 μm) produced by Dupont-Teijin were obtained from Tekra (New Berlin, WI). Exfoliated graphene nanoplatelets (GNP) (BET surface area: 300 m^2/gm and size 1 μm, and average thickness of 2–4 nm) were purchased from XG Sciences, Lansing, MI. All aqueous solutions were prepared using deionized (DI) water (>18.1 MΩ) supplied by a Barnstead Nanopure Diamond-UV purification unit equipped with a UV source and final 0.2 μm filter. Unless specified otherwise, all procedures were carried out at room temperature.

2.2. Layer-by-layer (LbL) assembly of polyelectrolyte modified GNP

For the hydrogen bonded assembly, the concentration of PAA and BPEI was adjusted to 2 mg/ml and 1 mg/ml, respectively. GNP platelets were dispersed in BPEI solution (now called BPEI-GNP) using a Fisher Scientific Ultrasonic probe (16 W) by sonicating for 1 h. GNP-BPEI solution was stirred overnight before use. The pH of the PAA and BPEI-GNP solution was adjusted to 4.0 and 7.5, respectively. For the deposition of the electrostatic layers, GNP were dispersed in 2 mg/ml BPEI solution using ultrasonication followed by magnetic stirring for at least 8 h. The excess polyelectrolyte is removed by passing the BPEI modified graphene solution through a 0.22 μm cellulose-acetate membrane-filter systems from Nalgene. The BPEI modified graphene platelets collected on the filter membrane were washed with copious quantity of DI water and subjected to another cycle of filtration. They are finally suspended in DI water, and the pH is adjusted to 3.5–3.8. The PAA solution used for electrostatic deposition (concentration: 2 mg/ml) was adjusted to a pH of 6.0. For the preparation of composite films, the desired number of hydrogen bonded bilayers was initially deposited. This was followed by the required number of electrostatic layers.

The LbL assembly was carried out using a customized Carl-Zeiss slide-stainer. Before depositing the multilayers, the surface of the polyester films was cleaned using a Harrick plasma cleaner (Harrick Scientific Corporation, Broading Ossining, NY). The films were subjected to air plasma for a period of 15 min. Air plasma helps in surface activation by producing hydrophilic moieties on the surface of the films. The immersion time was fixed to 15 min followed by a DI water rinse cycle of 2 min. After the deposition of each layer, the films were allowed to dry naturally for 5 min. After the

LbL process was complete, the films were heated in an oven maintained at 65 °C for 2 h to promote thermal cross-linking.

2.3. Multilayers characterizations

Multilayer films of GNP films on PET surface were characterized using scanning electron microscopy (SEM, JEOL 6610LV). The samples were cross-sectioned to reveal the thickness of the deposited films using a single edged razor blade that was cleaned with ethanol prior to use. The samples were coated with a thin layer of osmium for enhanced conductivity before SEM measurements. The surface resistance of multilayer films was measured with a Gamry Instruments Femtostat Station with frequency ranging from 1 to 10,000 Hz.

2.4. Oxygen transmission measurements

Oxygen barrier properties of films were tested in accordance with a MOCON 2/21 ML instrument (Mocon Inc., Minneapolis, MN, USA). The samples were tested at 0% relative humidity (RH) at a temperature of 23 °C.

3. Results and discussion

Hydrophilic polymers with numerous polar groups typically exhibit low specific free volume [56]. The polar groups can undergo hydrogen bonding producing a compact polymer structure that can prevent the permeation of gas molecules. The LbL assembly of BPEI and PAA is a pH driven process. These polymers form interpenetrating hydrogen bonded network when the terminal groups of the polymer chains exist in uncharged state [57]. The presence of impermeable material in the polymer matrix can further add to the gas barrier properties. Materials with high aspect ratio are generally preferred as fillers because of their ability to significantly increase the lag time for gas permeation through the polymer. Commercially available GNPs used in this study were prepared by using a unique non-oxidizing technology that enabled the platelets to retain their sp^2 configuration [58]. With an individual platelet thickness averaging 2 nm, and particle diameter of about 1–2 μm, the graphene nanoplatelets used in this study exhibit a significantly high aspect ratio increasing the chances of providing strong resistance to gas permeation. The elongated sheet-like geometry of graphene combined with high aspect ratio is also expected to achieve low percolation threshold value due to its ability to form a conducting network as compared to spherical or elliptical fillers [59]. However, the platelets have a tendency of stacking up reducing the effectiveness of using graphene as a high aspect ratio material. However, ultrasonication of graphene followed by continuous overnight stirring helps in improved dispersion of the nanoplatelets. The ultrasonication disrupts the stacking of the graphene platelets exposing individual platelets to BPEI functionalization. BPEI adsorbs on the graphene platelets due to hydrophobic interactions [52]. In case of negatively charged substrates, BPEI can assume a flat "pancake-like" structure as the cationic polymer segments in BPEI compensate the surface charges [60]. However in this case, the interaction between the neutral GNP and BPEI results in an optimized structure with bulky globular BPEI adsorbing on the surface of GNP. The polyelectrolyte modification minimizes graphene–graphene interaction improving the exfoliation of the platelets within the BPEI matrix. In our study, we tested three different LbL configurations of graphene embedded polyelectrolyte multilayers. The effect of these configurations on oxygen barrier properties and electrical sheet resistance has been shown in the subsequent sections. Mylar PET film about 76 μm thick was used as a base substrate in all cases.

3.1. Types of LbL deposited GnP/PEM films

The schematic diagram shown in Fig. 1 shows the three types of LbL assembly namely hydrogen bonded, electrostatic, and composite films. This section highlights the role played by adsorption

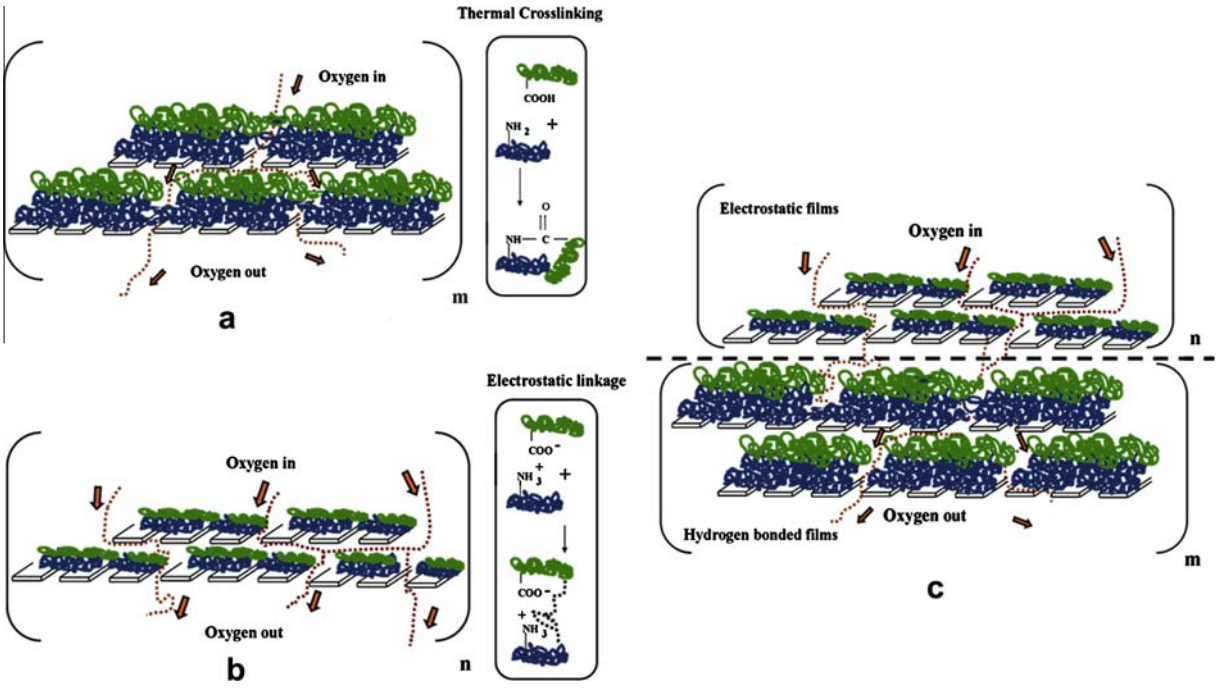

Fig. 1. Supramolecular assembly of graphene embedded polyelectrolyte multilayers. (a) Multilayers assembled using hydrogen bonded assembly. *m* denotes number of bilayers deposited. (b) Multilayers deposited using electrostatic interactions. *n* denotes the number of electrostatic bilayers deposited. (c) Composite film consisting of "*m*" number of hydrogen bonded bilayers followed by "*n*" number of electrostatic bilayers.

conditions to produce GNP/PEM films with specific type of interactions.

3.1.1. Hydrogen bonded films

Fig. 1a shows a schematic representation of the hydrogen bonded multilayers. *m* indicates the number of bilayers of hydrogen bonded graphene films deposited on the PET substrate. In this configuration, a multilayer assembly of BPEI-GNP and PAA was assembled on PET. The pH of the BPEI-GNP solution was adjusted to 7.5, whereas PAA was adjusted to 4.0. The native pH of BPEI-graphene is between 9.5 and 10.2. We observed that the BPEI-graphene solution when used in the LbL assembly without pH adjustment resulted in non-uniform coatings. We believe that the large difference between the pH values of BPEI-graphene and PAA solution can induce precipitation of certain charged groups in both the polyelectrolyte solutions leading to poor quality of LbL deposited film. The pK_a value for the primary and secondary amines in BPEI is approximately 4.5 and 6.7, respectively [61]. At a pH 7.5, most of the amine residues in BPEI should exist in uncharged state. The pK_a value of PAA is close to 4.8 [62]. Hence, at a pH 4.0, most of the terminal groups in PAA exist in uncharged state (carboxylic acid groups –COOH) rather than as carboxylate ion $–COO^-$. The presence of neutral terminal groups for both PAA and BPEI results in the deposition of highly coiled, loopy polyelectrolyte network. The interdiffusion of the polyelectrolyte segments followed by thermal cross-linking for 2 h at 65 °C gives rise to compact film architecture.

3.1.2. Electrostatically assembled films

Another type of LbL configuration was tested by retaining the same polyelectrolytes as before, except for two changes. The schematic representation of the same is shown in Fig. 1b. *n* denotes the number of electrostatic bilayers deposited. The deposition of BPEI-graphene solution during the LbL process represents a unique situation where both BPEI and polyelectrolyte modified graphene are competing for adsorption on the negatively charged PAA chains. Lu and co-workers [52] addressed this issue by subjecting the polyelectrolyte–graphene solution to vacuum filtration. By filtering the polyelectrolyte–graphene solution through 0.22 μm filter, Lu and co-workers removed the excess unbound

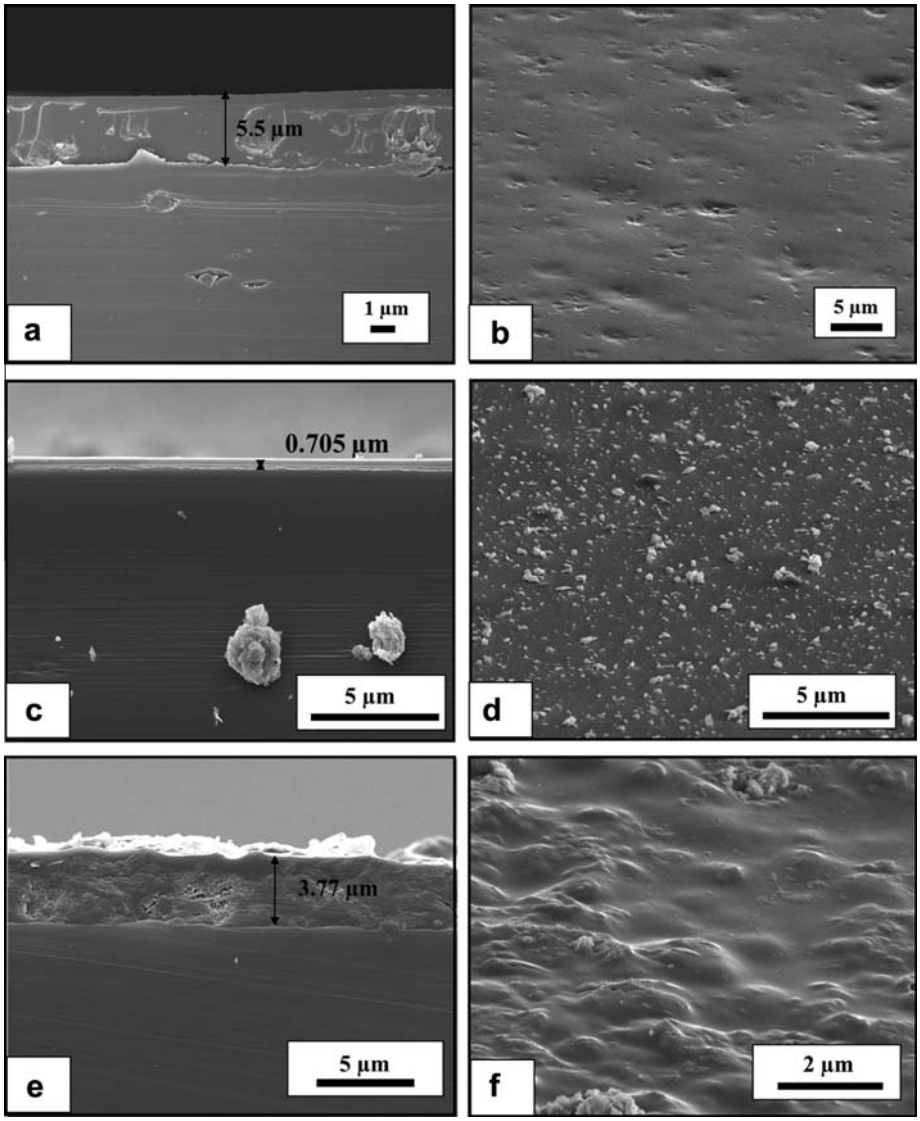

Fig. 2. SEM micrographs of 20 bilayer GNP embedded PEM assembly. a, c, e show sectional view of hydrogen bonded, electrostatic, and composite (10H + 10E) multilayers, respectively. Thickness of the coating is 5.5 μm, 0.705 μm, and 3.77 μm, respectively. b, d, f show surface morphology of hydrogen bonded, electrostatic, and composite films, respectively.

polyelectrolyte minimizing the ill-effects of competitive adsorption. The removal of non-conducting polyelectrolyte solution should also help in improved interconnection between individual graphene platelets. To counter the dense nature of the films produced in the earlier configuration, we implemented another change that targeted the interactions between the cationic and anionic components of the LbL assembly. The BPEI functionalized graphene after vacuum filtration was dispersed in DI water, and the pH was adjusted to 3.5–3.8. This pH value is lower than the pK_a value of the primary amines in BPEI (usually around 4.5). At this pH condition, the BPEI modified graphene platelets are positively charged. The BPEI chains that are functionalized on graphene platelets occur in protonated state ($-NH_3^+$). Meanwhile, the pH of PAA solution was adjusted to 6.0. This value is higher than the pK_a value of PAA. Thus, at this pH, PAA chains mostly exist in the ionized form. Though ionic cross-links are possible, the overall LbL assembly is governed by electrostatics.

3.1.3. Composite film

The synergistic combination of the above two systems is expected to deliver a result that includes contributions due to both hydrogen bonding and electrostatics, as shown in Fig. 1c. Using the same pH conditions as described before, a composite film consisting of the desired number of hydrogen bonded layers followed by electrostatic layers were deposited. The composite film is depicted as *m*H + *n*E where H and E stand for hydrogen bonded and electrostatic films, respectively.

3.2. Morphology and thickness of GNP embedded PEM films

The three types of LbL configurations listed above have distinct impact on the morphology and the thickness of the deposited films. Previous research has established that hydrogen bonded and electrostatically assembled PEMs can exhibit differences in morphology such as thickness and surface roughness [63,64]. Some of the hydrogen bonded multilayers are reported to exhibit an exponential growth pattern [65,66]. After a certain number of bilayers are deposited, these films may show linear increase in thickness [67]. Most electrostatic assemblies grow linearly [68] enabling easy estimation of thickness of individual bilayer. However, for exponential or hybrid (exponential + linear) growth regimes, the task is harder and requires more detailed analysis. In our case, the presence of graphene in the multilayer assembly can add complexity to the deposition process and influence the growth of these films. Though establishing the growth pattern of GNP embedded multilayers is not within the scope of this work, the morphology and thickness information about these films can provide useful insight into understanding the gas barrier and sheet resistance properties.

Fig. 2 shows SEM micrographs of the three LbL configurations for a 20 bilayer sample. The cross-sectional images (Fig. 2a, c and e) give an idea of the thickness of the multilayers, whereas Fig. 2b, d and f establish the surface morphology of these films. For the 20 bilayer sample under consideration, the thickness is highest for the hydrogen bonded assembly (about 5.5 μm). Electrostatic assembly results in thinner film (See Fig. 2c). With a thickness of around 705 nm, the electrostatic film is substantially thinner than the hydrogen bonded film. The composite film (Fig. 2e) has a thickness of 3.77 μm (lower than hydrogen bonded film but higher than electrostatically assembled multilayers). The other cases (4, 10, 15, and 30 bilayers samples) show similar thickness trend (See Supplementary Figs. S1, S2 and S3). The effect of the interactive forces associated with these configurations is evident from Fig. 2b, d and f. Fig. 2b shows surface morphology of 20 bilayer hydrogen bonded assembly. The surface is relatively smooth and free of graphene agglomerations. On the other hand, Fig. 2d shows the agglomerations of GNPs as a result of the electrostatic assembly. We suspect that the formation of aggregates is due to poor adhesion of BPEI functionalized graphene on the PET substrate. Hydrogen bonded films generally have good adhesive properties due to the presence of polar groups. A lower share of hydrogen bonding interactions in case of electrostatic films can reduce the adhesive capacity of the multilayers to hold the GNPs together. Fig. 2f shows the surface morphology of a composite film.

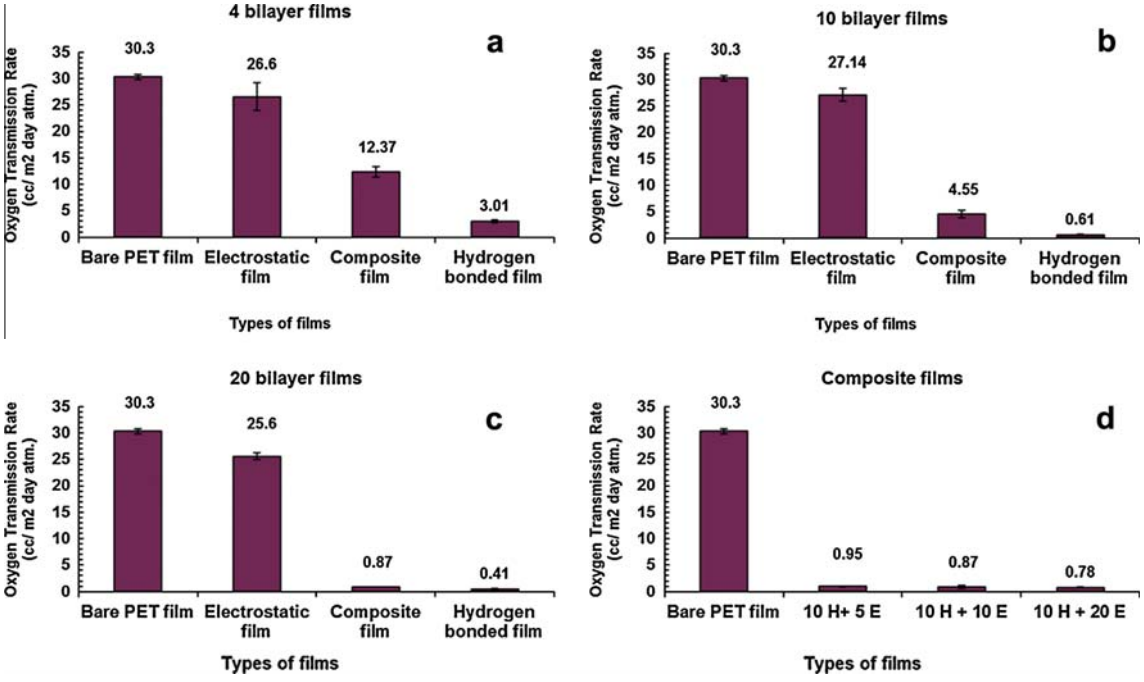

Fig. 3. Oxygen transmission rate (OTR) for different types of configurations. (a) Four bilayer system. The composite film consists of 2 hydrogen bonded and 2 electrostatic bilayers. (b) Ten bilayer system. Composite film consists of 5 hydrogen bonded and 5 electrostatic bilayers. (c) Twenty bilayer system. Composite film consists of 10 hydrogen bonded and 10 electrostatic bilayers. (d) Composite films consisting of 10 hydrogen bonded (H) followed by varying number of electrostatic (E) bilayers.

As expected, the surface morphology is a synergistic combination of the two assemblies shown previously. The surface has a certain texture resembling the hydrogen bonded films along with some degree of graphene agglomeration associated with electrostatic films. The adhesion provided by the underlying hydrogen bonded films facilitates good surface coverage by the electrostatic films. The improved interconnection between individual GNPs in the electrostatic layers promotes reduction in sheet resistance.

3.3. Oxygen barrier properties of GNP/PEM multilayers

Fig. 3a–d helps us compare the effect of hydrogen bonding, electrostatic, and composite interactions on the barrier properties of PET films. A bare PET film has an oxygen transmission rate (OTR) of 30.3 cc O_2/m^2 day atm. Deposition of just 4 bilayers of hydrogen bonded BPEI-graphene/PAA reduces the OTR by 90.07% (Fig. 3a). Measurements were also done after depositing 10 and 20 bilayers (See Fig. 3b and c). The OTR decreases as the number of bilayers increase. A 20 bilayer film (Fig. 3c) shows an impressive 98.6% reduction in the OTR value. The electrostatically assembled GNP/PEM films present a completely different result. Lack of hydrogen bonding can cause little or no significant reduction in the specific free volume greatly diminishing the ability of the graphene embedded film to function as effective oxygen barrier. A 20 bilayer electrostatic film exhibits a mere 14% reduction in OTR (Fig. 3c). Compared to electrostatic films, composite films display improved gas barrier properties (Fig. 3a–d). These films show a decreasing trend in OTR as the number of bilayers increased. When the deposition of hydrogen bonded layers reached 10, the OTR reduced by 98%. Increasing the number of electrostatic layers alone on hydrogen bonded films has little effect on the OTR values. This can be inferred from Fig. 3d where increasing the number of electrostatic layers (from 5 to 20) on fixed number of hydrogen bonded films results in a very small decrease in the OTR.

The SEM data from the previous section also provide critical information about film thickness that can be used for the estimation of the oxygen permeability coefficient. Unlike the OTR, the permeability coefficient takes into account the contribution of the thickness of the film and can provide useful information to compare different systems. For the calculation of film permeability coefficient, its contribution to the total permeability coefficient (inclusive of both the film as well as the PET substrate) was decoupled using a method described elsewhere [69]. Tables 1–4 show oxygen permeability coefficients for different LbL configurations at STP conditions. With thickness ranging from nanometers to few microns, the GNP/PEM films developed in this study show superior oxygen barrier properties compared to a 76.2 μm thick PET film. The graphene embedded PEM films show low permeability coefficients almost three orders of magnitude lower than the uncoated PET substrate (2433×10^{-18} cc cm/cm^2 s Pa). Since hydrogen bonded systems display the best oxygen barrier properties, a 20 bilayer hydrogen bonded BPEI/PAA system (without GNP) was assembled under the same pH conditions and its permeability coefficient was estimated to be 3.05×10^{-18} cc cm/cm^2 s Pa. However, the same result can be achieved by using just 4 bilayers of hydrogen bonded GNP/PEM multilayers assembled under similar deposition conditions. Among polymers, ethylene vinyl alcohol (EVOH) finds great application in the packaging industry on account of its low oxygen permeability. EVOH films with ethylene concentration ranging from 25 to 45 mol% are reported to exhibit enhanced gas barrier properties [70]. However, the GNP embedded hydrogen bonded and composite PEM films developed in this study have oxygen permeability coefficients that are at least 10 times lower than the permeability coefficient of a 15 μm thick EVOH film containing 44 mol% ethylene and about 1.4–3 times lower than the similarly sized EVOH film with 32 mol% ethylene [70]. The GNP/PEM films also show vastly superior oxygen barrier properties as compared to other graphene based nanocomposites reported in literature [49,71]. With permeability coefficient in the range of 10^{-18} cc cm/cm^2 s Pa, these coatings (hydrogen bonded and composite films) are comparable to SiO_2 thin films deposited on commercial gas barrier foils using plasma enhanced chemical vapor deposition (PECVD) technique [72]. Some important observations can be made from the data presented in Tables 1–4. Table 1 shows the effect of increasing number of hydrogen bonded GNP multilayers on oxygen permeability. While the total permeability coefficient (P_t) continues to register a drop, the permeability coefficient of the deposited film (P_f) increases slightly. This could be because the increase in the thickness of the coating negates the corresponding small drop in OTR. The data shown in Table 2 reinforce the poor barrier properties of electrostatic films. With increase in the number of bilayers, the data show no clear trend partly because of poor adhesion of the GNP multilayers in absence of uncharged polar groups. Table 3 shows a healthy decrease in P_f and P_t. The increasing number of hydrogen bonded multilayers facilitates a decrease in the permeability coefficient. Table 4 shows the effect of

Table 1
Oxygen permeability coefficient of hydrogen bonded films on PET substrate at STP conditions.

Number of bilayers	Thickness of the coating μm	Permeability coefficient (10^{-18} cc cm/cm^2 s Pa)	
		Film (P_f)	Total (P_t)
4 Bilayers	0.439	3.02	244.5
10 Bilayers	3.47	4.55	53.45
20 Bilayers	5.5	4.82	37.68

Table 2
Oxygen permeability coefficient of electrostatic films on PET substrate at STP conditions.

Number of bilayers	Thickness of the coating μm	Permeability coefficient (10^{-18} cc cm/cm^2 s Pa)	
		Film (P_f)	Total (P_t)
4 Bilayers	0.167	76.7	2146
10 Bilayers	0.455	25.2	2205
20 Bilayers	0.705	24.2	2094

Table 3
Oxygen permeability coefficient of composite films on PET substrate at STP conditions.

Number of bilayers	Thickness of the coating μm	Permeability coefficient (10^{-18} cc cm/cm^2 s Pa)	
		Film (P_f)	Total (P_t)
4 Bilayers	0.379	16.6	1003.4
10 Bilayers	0.893	10.1	374.03
20 Bilayers	3.77	7.12	76.79

Table 4
Oxygen permeability coefficient of composite films (variable electrostatic layers) on PET substrate at STP conditions.

Number of bilayers	Thickness of the coating μm	Permeability coefficient (10^{-18} cc cm/cm^2 s Pa)	
		Film (P_f)	Total (P_t)
10H + 5E	3.56	7.36	83.43
10H + 10E	3.77	7.12	76.70
10H + 20E	4.02	6.78	69.26

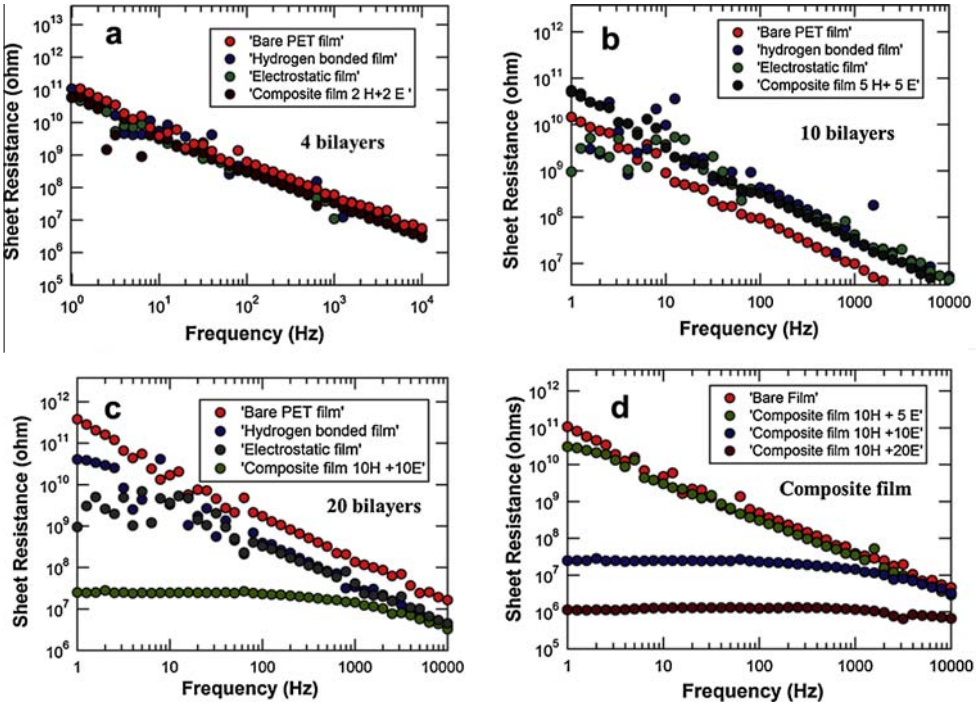

Fig. 4. Sheet resistance for different configurations of LbL assembled graphene embedded multilayers. Sheet resistance at 1 Hz for various samples is as follows: (a) Bare PET film: 111.1 GΩ, hydrogen bonded film: 108.2 GΩ, electrostatic film: 61.3 GΩ, composite film: 57.6 GΩ. (b) Bare PET film: 115.2 GΩ, hydrogen bonded film: 90.9 GΩ, electrostatic film: 54.3 GΩ, composite film: 50.2 GΩ. (c) Bare PET film: 110.2 GΩ, hydrogen bonded film: 40.8 GΩ, electrostatic film: 0.949 GΩ, composite film: 24.8 MΩ. (d) Bare PET film: 112.3 GΩ, composite film (10H + 5E): 31.2 GΩ, (10H + 10E): 24.8 MΩ, (10H + 20E): 1.14 MΩ.

increasing number of electrostatic films deposited on fixed number of hydrogen bonded films. Both P_t and P_f do not register a significant decrease which is consistent with our hypothesis that electrostatic films do not contribute to barrier properties.

3.4. Electrical resistance of the GNP/PEM multilayers

The electrical sheet resistance was also tested as a function of the number of bilayers. As seen from Fig. 4a, at 1 Hz, the electrical sheet resistance of the bare PET film is about 111.1 GΩ. The high value of resistance indicates that the film is highly resistive. The deposition of hydrogen bonded BPEI-graphene/PAA films reduces the resistance. The PET substrate shows a successive reduction in the resistance value for 4, 10, and 20 bilayers. For 20 bilayers, the value reduces to about 40.8 GΩ. Though there is a substantial reduction in the electrical resistance of the PET film, the values still end up in GΩ. We suspect that the high values of sheet resistance are a result of the dense network of hydrogen bonded polyelectrolytes surrounding the graphene platelets. The polymer wrapping of GNPs is known to reduce their conductivity.

Further, the loopy, coiled conformation of the polyelectrolytes prevents the interconnection between the individual graphene units limiting the electrical conductance of the film. As inferred from the SEM images, unlike the dense hydrogen bonded films, electrostatically assembled BPEI modified graphene/PAA films are substantially thinner. The combined effect of elimination of excess polyelectrolyte and thin film structure promotes further reduction in the electrical sheet resistance. As seen from Fig. 4c and a, 20 bilayer electrostatic films exhibit a sheet resistance of 0.95 GΩ. However, we suspect that further reduction in electrical resistance is hard to achieve due to poor adhesion of the multilayers to the substrate PET film. For the composite films, the electrical resistance drops further. Fig. 4d shows substantial reduction in the sheet resistance as the number of electrostatic layers is increased. The sheet resistance for a composite film consisting of 10 hydrogen bonded bilayers followed by 20 electrostatic bilayers drops to about 1.14 MΩ (Fig. 3d). This represents a five orders of magnitude reduction in sheet resistance. We believe that the composite film shows improved performance due to the synergistic effect of hydrogen bonded and electrostatic multilayers. Hydrogen bonded films have good adhesive properties due to presence of polar groups. The presence of hydrogen bonded films provides the adhesion to the electrostatic layers.

4. Conclusion

In summary, we showed the effect of three configuration types of graphene embedded polyelectrolyte systems. Hydrogen bonded graphene films showed good oxygen barrier property. Electrostatic films given their thin morphology and absence of excessive non-conducting polyelectrolyte exhibit lower sheet resistance. A composite film comprising of graphene embedded hydrogen bonded and electrostatic coatings satisfied both these requirements. The composite film showed oxygen permeability coefficient that is comparable to SiO_2 coatings with electrical sheet resistance five orders of magnitude lower than the base substrate. Besides the configurations described here, there is certainly more scope for improvement especially with respect to the electrostatic layers. The deposition process for the electrostatic layers comprising of BPEI modified graphene/PAA multilayers needs to be monitored for precipitation of charged groups. Being a pH sensitive system makes the solutions prone to sedimentation. This problem can be overcome by sonicating the BPEI modified graphene frequently (every 2 h) and adjusting the pH of the solutions in case of change. A more robust reproducible design can be obtained by casting films made from polystyrene sulfonate (PSS) functionalized graphene and a conjugate polycation such as poly(diallydimethylammonium chloride) (PDAC) which are less sensitive to pH changes. These

modifications may entail making suitable changes in the hydrogen bonded layers. Another parameter that significantly alters the morphology and potentially the conductivity of the coatings is the annealing temperature. The glass transition temperature (T_g) of PET is reported to be about 70 °C [73]. This has restricted the annealing temperature in our experiments to 65 °C. Higher temperatures generally contribute to increased cross-linking (improves gas barrier properties) and evaporation of moisture from the multilayers (facilitates improved conductivity). Using a polymer substrate with increased temperature tolerance can help achieve these objectives.

Acknowledgments

Financial support from the Department of Defense Strategic Environmental Research and Development Program (DOD SERDP W912HQ-12-C-0020), the USDA National Institute of Food and Agriculture (USDA-SBIR, 2011-33610-30822), and the MSU Foundation are greatly appreciated.

Appendix A. Supplementary material

Supplementary data associated with this article can be found, in the online version, at http://dx.doi.org/10.1016/j.jcis.2013.07.036.

References

[1] T. Ebina, F. Mizukami, Adv. Mater. 19 (2007) 2450–2453.
[2] C. Charton, N. Schiller, M. Fahland, A. Hollander, A. Wedel, K. Noller, Thin Solid Films 502 (2006) 99–103.
[3] A. Shirakura, M. Nakaya, Y. Koga, H. Kodama, T. Hasebe, T. Suzuki, Thin Solid Films 494 (2006) 84–91.
[4] K. Teshima, Y. Inoue, H. Sugimura, O. Takai, Vacuum 66 (2002) 353–357.
[5] A. Laaperi, Inf. Display 9 (2009) 09.
[6] A. Grill, W. Kane, J. Viggiano, M. Brady, R. Laibowitz, J. Mater. Res. 7 (1992) 3260–3265.
[7] A. Grill, C. Jahnes, C. Cabral, J. Mater. Res. 14 (1999) 1604–1609.
[8] G. Dennler, C. Lungenschmied, H. Neugebauer, N.S. Sariciftci, A. Labouret, J. Mater. Res. 20 (2005) 3224–3233.
[9] M. Jorgensen, K. Norrman, F.C. Krebs, Sol. Energy Mater. Sol. Cells 92 (2008) 686–714.
[10] C.-T. Chou, P.-W. Yu, M.-H. Tseng, C.-C. Hsu, J.-J. Shyue, C.-C. Wang, F.-Y. Tsai, Adv. Mater. 25 (2013) 1750–1754.
[11] N. Inagaki, S. Tasaka, M. Makino, J. Appl. Polym. Sci. 64 (1997) 1031–1039.
[12] N.K. Lape, E.E. Nuxoll, E.L. Cussler, J. Membr. Sci. 236 (2004) 29–37.
[13] J.P. DeRocher, B.T. Gettelfinger, J.S. Wang, E.E. Nuxoll, E.L. Cussler, J. Membr. Sci. 254 (2005) 21–30.
[14] L.E. Nielsen, J. Macromol. Sci. – Chem. 1 (1967) 929–942.
[15] O. Gain, E. Espuche, E. Pollet, M. Alexandre, P. Dubois, J. Polym. Sci. Part B: Polym. Phys. 43 (2005) 205–214.
[16] M.A. Priolo, D. Gamboa, K.M. Holder, J.C. Grunlan, Nano Lett. 10 (2010) 4970–4974.
[17] J.C. Grunlan, A. Grigorian, C.B. Hamilton, A.R. Mehrabi, J. Appl. Polym. Sci. 93 (2004) 1102–1109.
[18] V.D. Alves, N. Costa, I.M. Coelhoso, Carbohydr. Polym. 79 (2010) 269–276.
[19] M.D. Sanchez-Garcia, L. Hilliou, J.M. Lagaron, J. Agric. Food Chem. 58 (2010) 6884–6894.
[20] Q. Yang, H. Fukuzumi, T. Saito, A. Isogai, L. Zhang, Biomacromolecules 12 (2011) 2766–2771.
[21] C. Aulin, M. Gallstedt, T. Lindstrom, Cellulose 17 (2010) 559–574.
[22] H.-D. Huang, P.-G. Ren, J. Chen, W.-Q. Zhang, X. Ji, Z.-M. Li, J. Membr. Sci. 409–410 (2012) 156–163.
[23] A.A. Gokhale, J. Lu, I. Lee, J. Mol. Catal. B: Enzym. 90 (2013) 76–86.
[24] H. Kim, Y. Miura, C.W. Macosko, Chem. Mater. 22 (2010) 3441–3450.
[25] A.K. Geim, Science 324 (2009) 1530–1534.
[26] R.K. Iler, J. Colloid Interface Sci. 21 (1966) 569–594.
[27] G. Decher, J.D. Hong, Makromol. Chem.– Macromol. Symp. 46 (1991) 321–327.
[28] G. Decher, J.D. Hong, Ber. Bunsen-Ges. – Phys. Chem. Chem. Phys. 95 (1991) 1430–1434.
[29] I. Lee, Langmuir 29 (2013) 2476–2489.
[30] T.R. Hendricks, E.E. Dams, S.T. Wensing, I. Lee, Langmuir 23 (2007) 7404–7410.
[31] A.M. Yu, Y.J. Wang, E. Barlow, F. Caruso, Adv. Mater. 17 (2005) 1737–1741.
[32] Y. Lvov, F. Caruso, Anal. Chem. 73 (2001) 4212–4217.
[33] W.Q. Shan, P. Bacchin, P. Aimar, M.L. Bruening, V.V. Tarabara, J. Membr. Sci. 349 (2010) 268–278.
[34] D.M. Dotzauer, J.H. Dai, L. Sun, M.L. Bruening, Nano Lett. 6 (2006) 2268–2272.
[35] B.L. Hassler, N. Kohli, J.G. Zeikus, I. Lee, R.M. Worden, Langmuir 23 (2007) 7127–7133.
[36] S. Devesh, K. Neeraj, J.R. Rudy, M.W. Robert, L. Ilsoon, Neuropathy Target Esterase Biosensor, in: Vernon S. Somerset (Ed.), INTECH: Intelligent and Biosensors, 2010.
[37] J. Lu, L.T. Drzal, R.M. Worden, I. Lee, Chem. Mater. 19 (2007) 6240–6246.
[38] J. Lu, I. Do, L.T. Drzal, R.M. Worden, I. Lee, Acs Nano 2 (2008) 1825–1832.
[39] K. Sambanthamoorthy, A.A. Gokhale, W.W. Lao, V. Parashar, M.B. Neiditch, M.F. Semmelhack, I. Lee, C.M. Waters, Antimicrob. Agents Chemother. 55 (2011) 4369–4378.
[40] S. Mehrotra, D. Lynam, R. Maloney, K.M. Pawelec, M.H. Tuszynski, I. Lee, C. Chan, J. Sakamoto, Adv. Funct. Mater. 20 (2010) 878.
[41] S. Mehrotra, I. Lee, C. Chan, Acta Biomater. 5 (2009) 1474–1488.
[42] S. Mehrotra, D. Lynam, C. Liu, D. Shahriari, I. Lee, M. Tuszynski, J. Sakamoto, C. Chan, J. Biomater. Sci. – Polym. E 23 (2012) 439–463.
[43] S.L. Clark, M.F. Montague, P.T. Hammond, Macromolecules 30 (1997) 7237–7244.
[44] S.Y. Yang, M.F. Rubner, J. Am. Chem. Soc. 124 (2002) 2100–2101.
[45] T.R. Hendricks, W. Wang, I. Lee, Soft Matter 6 (2010) 3701–3706.
[46] T.R. Hendricks, I. Lee, Nano Lett. 7 (2007) 372–379.
[47] S. Biswas, H. Fukushima, L.T. Drzal, Compos. Part A – Appl. Sci. Manuf. 42 (2011) 371–375.
[48] Fukushima, H. Graphite nanoreinforcements in polymer nanocomposites, PhD Dissertation, Department of Chemical Engineering and Materials Science, Michigan State University, East Lansing, MI, USA, (2003).
[49] H. Wu, L.T. Drzal, Carbon 50 (2012) 1135–1145.
[50] X. Jiang, L.T. Drzal, J. Appl. Polym. Sci. 124 (2012) 525–535.
[51] T.R. Hendricks, J. Lu, L.T. Drzal, I. Lee, Adv. Mater. 20 (2008) 2008–2012.
[52] J. Lu, I. Do, H. Fukushima, I. Lee, L.T. Drzal, J. Nanomater. 2010 (2010) 2.
[53] S.S. Shiratori, M.F. Rubner, Macromolecules 33 (2000) 4213–4219.
[54] H.M. Kim, J.K. Lee, H.S. Lee, Thin Solid Films 519 (2011) 7766–7771.
[55] L. Yu, Y.S. Lim, J.H. Han, K. Kim, J.Y. Kim, S.Y. Choi, K. Shin, Synth. Met. 162 (2012) 710–714.
[56] C. Nagel, K. Gunther-Schade, D. Fritsch, T. Strunskus, F. Faupel, Macromolecules 35 (2002) 2071–2077.
[57] Y.H. Yang, M. Haile, Y.T. Park, F.A. Malek, J.C. Grunlan, Macromolecules 44 (2011) 1450–1459.
[58] http://xgsciences.com/wp-content/uploads/2012/09/About-xGnP.pdf, in.
[59] S. Kim, I. Do, L.T. Drzal, Macromol. Mater. Eng. 294 (2009) 196–205.
[60] M. Schneider, M. Brinkmann, H. Mohwald, Macromolecules 36 (2003) 9510–9518.
[61] I. Willner, Y. Eichen, A.J. Frank, M.A. Fox, J. Phys. Chem. 97 (1993) 7264–7271.
[62] S. Bequet, T. Abenoza, P. Aptel, J.M. Espenan, J.C. Remigy, A. Ricard, Desalination 131 (2000) 299–305.
[63] J.F. Quinn, A.P.R. Johnston, G.K. Such, A.N. Zelikin, F. Caruso, Chem. Soc. Rev. 36 (2007) 707–718.
[64] P. Lavalle, C. Gergely, F.J.G. Cuisinier, G. Decher, P. Schaaf, J.C. Voegel, C. Picart, Macromolecules 35 (2002) 4458–4465.
[65] D.M. DeLongchamp, P.T. Hammond, Langmuir 20 (2004) 5403–5411.
[66] C. Picart, P. Lavalle, P. Hubert, F. Cuisinier, G. Decher, P. Schaaf, J.-C. Voegel, Langmuir 17 (2001) 7414–7424.
[67] A. Laachachi, V. Ball, K. Apaydin, V. Toniazzo, D. Ruch, Langmuir 27 (2011) 13879–13887.
[68] J.-A. He, L. Samuelson, L. Li, J. Kumar, S.K. Tripathy, Langmuir 14 (1998) 1674–1679.
[69] H. Chatham, Surf. Coat. Technol. 78 (1996) 1–9.
[70] Z.B. Zhang, I.J. Britt, M.A. Tung, J. Appl. Polym. Sci. 82 (2001) 1866–1872.
[71] K. Kalaitzidou, H. Fukushima, L.T. Drzal, Carbon 45 (2007) 1446–1452.
[72] J. Jiang, M. Benter, R. Taboryski, K. Bechgaard, J. Appl. Polym. Sci. 115 (2010) 2767–2772.
[73] G.S. Fielding-Russell, P.S. Pillai, Makromol. Chem. 135 (1970) 263–274.